Coulomb interaction and transport in tunnel junctions and quantum dots

T. Brandes, W. Häusler, K. Jauregui, B. Kramer and D. Weinmann[1]

Physikalisch-Technische Bundesanstalt, Braunschweig, Germany

In the first part of the paper the AC conductance of a quasi-one-dimensional tunnel junction involving a potential barrier is calculated in linear response. Its frequency dependence is used to define a dynamical capacitance. The influence of phase breaking electron–phonon interactions is investigated. It is argued that Coulomb interaction is of minor importance at higher frequencies and that dynamic and static capacitances are the same. The argument provides a high-frequency limit for turnstile operation. In the second part, the quantum mechanical properties of few interacting electrons in quantum dots are considered. Including the spin degree of freedom, the spectral properties of up to four interacting electrons confined within a quasi-one-dimensional system of finite length with Coulomb interactions are investigated by numerical diagonalization. The limitations of the description in terms of a capacitance are discussed. For sufficiently low density the electrons become localized, forming a Wigner molecule. The energetically lowest excitations are identified as vibrational and tunneling modes, both being collective modes involving all the electrons.

1. Introduction

Interaction effects play a crucial role in the understanding of the electronic transport properties of very small condensed matter systems at low temperatures [1]. Examples are

- the Coulomb blockade [2,3], where charging energies of single electrons suppress the current through a dissipatively shunted tunnel junction;
- single electron tunneling (SET) oscillations [4] of the voltage across a tunnel junction at constant current;
- resonance-like oscillations of the conductance of quantum dots, being periodic in multiples of the elementary charge inside the dot [5–7].

An important feature in conductance measurements involving tunnel junctions and quantum dots is the relative isolation of the sample region from the 'external world'. In the Coulomb blockade experiments this is achieved by a shunt impedance representing the (phase randomizing) influence of a coupling to the electromagnetic environment. In the quantum dot experiments, weak coupling is achieved by almost impenetrable tunnel junctions. Here the time scale for a tunneling event is large compared to the other inverse energies involved, namely the Fermi energy of the external wires, the charging energy and the characteristic energy of the dissipative heat bath. On the time scale of all relaxation processes, the electron number becomes a good quantum number. The quantum properties of the disconnected dot can therefore be considered as the most dominating factor in the single electron phenomena. The Coulomb interaction should be taken into account because the charging energy is the most relevant energy scale of the problem. The validity of the commonly used phenomenological description by means of the classical concept of a capacitance C [8,9] is not completely obvious [10,11] and needs to be justified.

In this paper, we investigate the question of the justification of the capacitance in very small quantum systems by considering their dynamical

Correspondence to: T. Brandes, Physikalisch-Technische Bundesanstalt, Bundesallee 100, W-3300 Braunschweig, Germany.

[1] On leave from: II. Institut für Theoretische Physik, Universität Stuttgart, 7000 Stuttgart 80, Germany.

and statical properties. In section 2 the AC conductance of a quasi-one-dimensional potential barrier is calculated and interpreted in terms of a dynamical capacitance, which is found to be relevant at higher frequencies. We demonstrate that it is completely determined by the quantum mechanical properties of the system by considering the influence of phase breaking electron–phonon interaction. In section 3 a model of few Coulombically interacting electrons within a 1D square well potential is examined. We clarify the competition between confinement energy and Coulomb interaction [12] for low electron numbers [7,13] and for dilute electron systems. Two kinds of elementary excitations, *vibrational* and *tunneling* modes are identified. They are characteristic for the region of dilute and intermediate electron densities and can be understood physically in terms of the *Wigner molecule* picture.

2. AC conductance and dynamical capacitance of tunnel junctions

2.1. Frequency-dependent transport

Using the frequency-dependent conductance one can define a capacitance of a tunnel junction modeled by a potential barrier without referring to the Coulomb energy. We will demonstrate that in certain regions of Fermi energy E_F and barrier parameters one can simulate the behavior of the quantum system by a circuit involving resistors and a capacitor. The 'dynamical' capacitance defined in this way is a genuine quantum feature. This is demonstrated by studying the dependence of the AC conductance on inelastic processes using a simplified model involving electron–phonon coupling. The capacitive behavior is suppressed as temperature is increased when inelastic scattering is present. A similar effect has been found recently [14] using a semi-classical approach yielding the current–voltage characteristic at zero frequency.

In the following we use quantum mechanical linear response theory. It provides a formalism that allows, at least in principle, to treat inelastic processes and interactions in a systematic manner.

For simplicity, the electric field $E(x, t) = E_0\, \Theta(l/2 - |x|) \cos(\omega t)$ is assumed to be constant on a finite interval l of an infinitely long wire. The conductance $\Gamma(\omega)$, defined via the absorbed power [15,16], is given by the spatial average of the real (absorptive) part of the conductivity

$$\Gamma(\omega) = \frac{1}{l^2} \int_{-l/2}^{l/2} \mathrm{d}x\, \mathrm{d}x'\, \mathrm{Re}\, \sigma(x, x'; \omega)\,. \qquad (1)$$

In order to decide whether or not the dynamical capacitance is the same as the static capacitance needed to understand Coulomb blockade it is in principle necessary to consider the influence of electron–electron interaction. While Coulomb interactions are crucial in the case of zero frequency, their importance for the conductance diminishes as frequency is increased. This can be concluded from the RPA result for the density–density correlation function [17] of a quantum wire where the interaction-induced corrections to the non-interacting limit vanish as ω^{-2}.

A quantitative estimate of the frequency ω_0 above which Coulomb interactions have minor influence can be found using the tunneling Hamiltonian

$$H = H_L + H_R + H_T + H_C\,,$$

where H_L and H_R describe semi-infinite wires on the left and right side of the barrier. They are coupled by the tunneling term H_T and the Coulomb interaction modeled by $H_C = \lambda(Q_L - Q_R)^2$, where Q_L and Q_R are the total charge in the left and the right wire and λ parametrizes the interaction strength. Applying linear response theory for $\lambda = 0$, one finds that the conductance consists of two contributions. The first is $\Gamma_{si} = (e^2/h)(\omega l/4v_F)^2$ at low frequencies $\hbar\omega \ll E_F$ and $k_F l \gg 1$ and is due to the motion of the electrons in the semi-infinite wires. Here, l is the interval where the electric field is applied, v_F and k_F are

the Fermi velocity and wave vector, respectively. The second contribution is the DC value $(e^2/h)T$, which is due to electrons tunneling through the barrier with transmission probability T. Taking into account the Coulomb interaction ($\lambda \neq 0$), the first contribution remains unchanged and H_C results only in a constant energy shift. The second contribution to Γ arising from charge-changing tunneling turns out to be suppressed [18]. We define ω_0 as the frequency above which the unchanged term $\sim\omega^2$ prevails over the (DC-) contribution at $\lambda = 0$ that is influenced by Coulomb interactions. Well above this frequency, which is given by $\omega_0 = (4v_F/l)\sqrt{T}$, the total conductance is dominated by the semi-infinite wires, independent of the strength of the interaction λ. For high frequencies $\omega \gg \omega_0$ the investigation of frequency dependent transport properties of tunnel junctions neglecting electron–electron interactions should be a good approximation for the system even in the presence of interactions.

2.2. *The model system*

Instead of the tunneling Hamiltonian including Coulomb interaction, we consider now a quasi-one-dimensional system confined by a parabolic potential in transversal direction without Coulomb interaction. A rectangular potential barrier of length b and height V in the longitudinal direction serves as a model for a tunnel junction. This description is more suitable for a discussion of the dependence on barrier parameters than the tunneling Hamiltonian. We solve the Schrödinger equation with the potential $V(x, x_\perp) = V\Theta(b/2 - |x|) + V(x_\perp)$ and assume that the wire is narrow enough to allow the restriction to the lowest band with transversal wave function $\chi(x_\perp) \sim \exp -(x_\perp/2\lambda)^2 (x = (x, x_\perp))$, where λ is the effective transversal width. For a system of total length L we calculate the exact longitudinal eigenfunctions using periodic boundary conditions at $x = \pm L/2$ and evaluate the conductance for $L \to \infty$. The result is

$$\Gamma(\omega) = \frac{h}{2l^2} \int_0^\infty \mathrm{d}E \, \frac{f(E) - f(E + \hbar\omega)}{\hbar\omega} \times \left(\frac{mL}{2\pi\hbar^2}\right)^2 \frac{1}{kk_\omega} (|J^{sa}_{kk_\omega}|^2 + |J^{sa}_{k_\omega k}|^2) ,$$

with $k = [2mE]^{1/2}/\hbar$ and $k_\omega = [2m(E + \hbar\omega)]^{1/2}/\hbar$ (m effective mass). The current matrix elements between symmetrical states characterized by the wave number k_1 and antisymmetric states that correspond to k_2 are

$$J^{sa}_{k_1k_2} = \frac{e\hbar}{imL} (\Theta(l - b)[\xi_{k_1k_2}(l) - \xi_{k_1k_2}(b)] + \gamma^s_{k_1}\gamma^a_{k_2}\zeta_{k_1k_2}(b)) .$$

Here, we have introduced the functions

$$\xi_{k_1k_2}(x) = \cos[k^- x/2 + \phi^-]k^+/k^- - \cos[k^+ x/2 + \phi^+]k^-/k^+ ,$$

$$\zeta_{k_1k_2}(x) = \sinh[\kappa^+ x/2]\kappa^-/\kappa^- , - \sinh[\kappa^- x/2]\kappa^+/\kappa^- ,$$

with $\kappa_{1,2} = [2mV/\hbar^2 - k^2_{1,2}]^{1/2}$ $(k^\pm = k_1 \pm k_2$, $\kappa^\pm = \kappa_1 \pm \kappa_2$, $\phi^\pm = \phi^s_{k_1} \pm \phi^a_{k_2})$. The factors $\gamma^{s,a}_k$ describe the suppression of the wave function under the barrier and the angles $\phi^{s,a}_k$ are connected with the phase shift of the wave functions. $\Gamma(\omega)$ at zero temperature is plotted in fig. 1 for various values of E_F.

It is instructive to consider some limiting cases: For $V = 0$ or $b = 0$, the well known [16] conductance of a free quantum wire in the regime $\hbar\omega \ll E_F$ is reproduced,

$$\Gamma_{free}(\omega) = \frac{e^2}{h} \left(\frac{\sin(\omega l/2v_F)}{\omega l/2v_F}\right)^2 . \qquad (2)$$

By means of the Kramers–Kronig relation, one obtains from the real (absorptive) part (2) an approximation for the imaginary (reactive) part

$$\Gamma'_{free}(\omega) = \frac{e^2}{h} \frac{2v_F}{\omega l} \left(1 - \frac{\sin(\omega l/v_F)}{\omega l/v_F}\right) , \qquad (3)$$

which is correct at low frequencies. The behavior

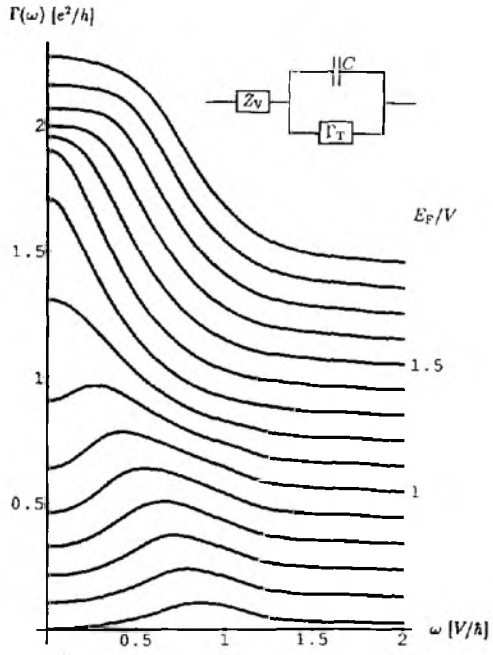

Fig. 1. AC conductance of the one-dimensional system with a barrier of length $b = 5\hbar(2mV)^{-1/2}$ and field length $l = 7\hbar(2mV)^{-1/2}$ at zero temperature for various values of E_F (the curves are offset). The inset shows the classical circuit to simulate the AC behavior of the tunnel junction.

of $\Gamma_{free}(\omega)$ is very close to the conductance of a classical resistance h/e^2 and an inductance $(h/e^2)l/3v_F$ in series.

The limit $\omega \to 0$ gives $\Gamma_{DC} = (e^2/h)T(E_F)$ with the transmission coefficient of the barrier $T(E_F)$. Thus, the Landauer formula [19] is identical to the DC limit of linear response theory [20]. Due to the presence of quantum coherence this result is independent of the region where the driving field is applied, even if it is completely outside the barrier.

For a nearly impenetrable barrier, keeping only the leading term in $\exp(-\kappa b)$ we expand with respect to ω for $k_F \ll \kappa_F$ and find for the simplest case $b = l$ (details for the general case will be given elsewhere [18])

$$\Gamma(\omega) = \frac{e^2}{h} T(E_F) + \frac{e^2 m^2}{2\pi\hbar^3 b^2} \frac{k_F^2}{\kappa_F^8} \omega^2 + O[\omega^4] . \quad (4)$$

The second term may be interpreted in terms of a capacitance: we consider a classical circuit (fig. 1) and expand the real part of its conductance for low frequencies. In the case $\Gamma_T \ll 1/|Z_V|$, using for the impedance Z_V the results for the free quantum wire (2) and (3), we find

$$\Gamma_c(\omega) = \Gamma_T + \frac{h}{e^2} C^2 \omega^2 + O[\omega^4] .$$

Comparison with eq. (4) yields

$$C = \frac{e^2 m}{2\pi\hbar^2} \frac{k_\Gamma}{\kappa_F^4} \frac{1}{b} .$$

Using reasonable values of the parameters, suitable for instance for GaAs–AlGaAs heterostructures [6], we find that a barrier of length $b \approx 130$ nm and height 0.75 meV has a capacitance of the order of 10^{-18} F per conductance channel at $E_F = 0.05$ meV. Furthermore, we see that the critical frequency ω_0, below which the influence of electron–electron interactions is of importance, is very small on the frequency scale $V/\hbar$ characteristic for the AC conductance at low frequencies. Therefore the low frequency expansion remains valid well above ω_0. For a wire of finite width the number of channels increases proportional to the cross-section A of the wire and $C \sim A/b$ as for a classical parallel-plate capacitor, when the potential representing the tunnel junction is independent of the transverse coordinates.

We want to emphasize that the capacitance discussed above describes the behavior of the tunnel junction at high frequencies and is not a correction to the static capacitance like the one due to quasiparticle tunneling in Josephson junctions as calculated in ref. [10].

2.3. The influence of inelastic processes

To demonstrate that the capacitive behavior (4) is of quantum mechanical origin we investigate the influence of inelastic processes. We will see that they eventually lead to a vanishing of the effect.

We consider a simplified version of the above model, namely a barrier of the form $V(x) =$

$V_0\delta(x)$. The (retarded) single-electron Green's function is [21]

$$G(x, x'; \omega) = G^0(x, x'; \omega) + \frac{V_0}{1 - V_0 G^0(0, 0; \omega)} G^0(x, 0; \omega) \times G^0(0, x'; \omega) ,$$

where G^0 is the Green's function for $V_0 = 0$. The simplest approach to take into account phase breaking processes consists in renormalizing G^0 by a self-energy Σ caused by electron–phonon (e–p) interaction. We assume that electrons and phonons are coupled via a deformation potential [17]

$$V_{e-p}(x) = \frac{1}{\sqrt{\Omega}} \sum_Q V_Q F(Q_\perp) \exp(iqx)(a_Q + a^+_{-Q}) ,$$

with phonon wave vector $Q = (q, Q_\perp)$, $|V_Q|^2 = V_D^2 |Q| / Q_D^4$, Debye cutoff Q_D and coupling parameter V_D, Ω being the total system volume ($\Omega \to \infty$). The form factor $F(Q_\perp) = \langle \chi | \exp(iQ_\perp x_\perp) | \chi \rangle$ reflects the fact that although the phonons are three-dimensional the e–p coupling is affected by the confining potential. In second order perturbation theory with respect to e–p coupling and close to E_F, we can restrict ourselves to $\operatorname{Im} \Sigma(k, \omega)$, numerical evaluation yielding only weak k- but strong ω-dependence around E_F similar to the results of ref. [22]. Neglecting the k-dependence of Σ around the Fermi wave vector k_F we get

$$G^0 = -\frac{im}{\hbar^2 \gamma(\omega)} \exp(i\gamma(\omega)|x - x'|) ,$$

$$\gamma(\omega) = \sqrt{\frac{2m}{\hbar^2} (\hbar\omega + E_F - i \operatorname{Im} \Sigma(k_F, \omega))} ,$$

from which we calculate G and the corresponding spectral function $-(1/\pi) \operatorname{Im} G$. Neglecting vertex corrections, the dissipative nonlocal conductivity of the one-channel system can be calculated from the Kubo formula involving only products of the spectral functions at different energies [23].

From the general result (1) one finds the DC limit of the conductance. The e–p interaction introduces an additional length-scale, namely $l_{in}^{-1} := 2 \operatorname{Im}[2m/\hbar^2 (E_F - i \operatorname{Im} \Sigma(k_F, 0))]^{1/2}$ which is the decay-length of the Green's function G^0 without the barrier. We evaluate the DC resistance $R = \Gamma^{-1}(0)$ as a function of l/l_{in} for $k_B T \ll E_F$ and $k_F l_{in} \gg 1$ corresponding to weak e–p coupling (fig. 2). For $l_{in} = \infty$ we reproduce Landauer's result, for $l/l_{in} \gg 1$ we have ohmic behavior with R proportional to the effective length l of the wire. In the intermediate region the behavior of R depends on the δ-barrier strength V_0.

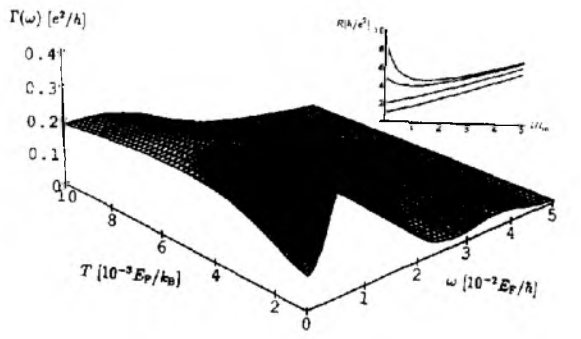

Fig. 2. Conductance $\Gamma(\omega)$ for δ-barrier strength $k_F V_0 / E_F = 7$ and $k_F l = 1000$. Self-energy parameters are $(V_D/E_F)^2 = 0.08\pi$, $Q_D/k_F = 1$, $\hbar\omega_D/E_F = 0.01$ and $k_F \lambda = 1$. In the inset, the resistance at $\omega = 0$ for δ-barrier strength $k_F V_0 / E_F = 0, 2, 4, 6$ (from below) is shown as a function of l/l_{in}.

The evaluation of $\Gamma(\omega)$ (fig. 2) at nonzero frequency is again simplified when $\omega \ll E_F/\hbar$ besides $k_B T \ll E_F$. The increase of conductance with frequency for small ω can again be interpreted as a capacitive behavior. The oscillatory decrease of $\Gamma(\omega)$ is similar to the free one-channel quantum wire (2).

The most important result is the suppression of oscillatory and capacitative behavior with increasing temperature as a result of the loss of phase coherence. Both effects are destroyed the e–p interaction showing that the dynamical capacitance is a quantum mechanical property of the system.

3. Interacting electrons in quantum dots

In order to investigate the quantum mechanical meaning of a static capacitance we consider

numerically the influence of the Coulomb interaction on a few electrons in a 1D square well potential. In contrast to previous work [24] we treat up to $N = 4$ electrons exactly.

3.1. Model of a square well potential

For the electron–electron interaction, we use a potential

$$V(x, x') \propto \frac{1}{\sqrt{(x - x')^2 + \lambda^2}}, \tag{5}$$

which behaves Coulombically at large distances. λ is a measure for the width of the electron wave functions in transversal direction. In most of our calculations we take $\lambda/L = 2 \times 10^{-4} \ll 1$, where L is the system length. Then, the eigenvalues of the Hamiltonian

$$H = E_{\mathrm{H}} \frac{a_{\mathrm{B}}}{L} \left(\frac{a_{\mathrm{B}}}{L} H_0 + H_1 \right) \tag{6}$$

depend only weakly on λ. $E_{\mathrm{H}} = e^2/a_{\mathrm{B}}$ is the Hartree energy, $a_{\mathrm{B}} = \varepsilon \hbar^2/me^2$ the Bohr radius, ε the relative dielectric constant and m the effective electron mass. The relative importance of the kinetic energy in the 1D square well potential

$$H_0 = \sum_{n,\sigma} \epsilon_n c^{\dagger}_{n,\sigma} c_{n,\sigma}$$

($\varepsilon_n \propto n^2$, $n \in \mathbb{N}$) decreases as compared to the Coulomb energy

$$H_1 = \sum_{n_1 \ldots n_4, \sigma_1, \sigma_2} V_{n_4 n_3 n_2 n_1} c^{\dagger}_{n_4 \sigma_1} c^{\dagger}_{n_3 \sigma_2} c_{n_2 \sigma_2} c_{n_1 \sigma_1}, \tag{7}$$

with increasing system length L. The matrix elements $V_{n_4 n_3 n_2 n_1}$ are real and do not depend on the electron spin σ. The total spin S is therefore conserved and all eigenvalues are $(2S + 1)$-fold degenerate.

We want to discuss the interplay between kinetic energy H_0 and Coulomb energy H_1 as function of system length and electron number. No charge neutralizing background [11] is taken into account. It would be only relevant to study the influence of a selfconsistent adjustment of the background charge distribution with varying the electron number (the total background charge in the experiment is regulated externally by the gate voltage). Such contributions should not modify our results qualitatively.

For the numerical diagonalization single particle states $c^{\dagger}_{n\sigma}|0\rangle$ with $1 \leqslant n \leqslant M$ were chosen (usually $M = 9 \ldots 17$, depending on the calculation). The properly anti-symmetrized, non-interacting N-particle basis $\psi^{(N)}_{\nu}$, including the spin degree of freedom, is of dimensionality

$$R = \binom{2M}{N}, \quad 1 \leqslant \nu \leqslant R.$$

In our calculations R was restricted to 1.5×10^4, even when using Lanczos procedures. To avoid loops over all R^2 matrix elements of the Hamiltonian, we used the following economic procedure to occupy the matrix. Starting from the $(N-2)$-particle basis, the application of two creation operators onto a certain $\psi^{(N-2)}_{\mu}$ generates say the N-particle state $\psi^{(N)}_{\nu}$ with proper sign. $\psi^{(N)}_{\nu}$ corresponds to a certain row ν of the Hamiltonian matrix. Creating from the same $\psi^{(N-2)}_{\mu}$ a (different or the same!) $\psi^{(N)}_{\nu'}$ identifies a certain column ν'. The *independent* summation over all possible two-particle excitations and

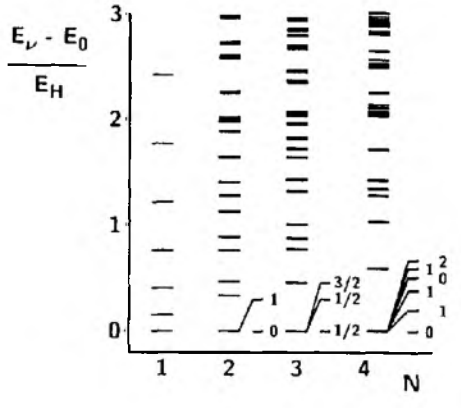

Fig. 3. Typical spectra of model (6) for various N and $L = 9.45 a_{\mathrm{B}}$. For $N \geqslant 2$ the low lying eigenvalues form groups of (fine structure) multiplets, the total number of states per multiplet being equal to the dimensionality of the spin Hilbert space 2^N. This is shown in the magnification. The ground state energy is subtracted respectively.

subsequent summation over all $(N-2)$-particle states generates eventually all non-vanishing entries (including sums from $n_4 = n_1$ and/or $n_3 = n_2$, cf. eq. (7)) of the Hamiltonian matrix.

Typical examples of N-electron energy spectra are shown in fig. 3. In presence of interaction, $N > 1$, the density of states becomes much more inhomogeneous. The lowest eigenvalues form *multiplets* of extremely small width when $L \gg Na_B$. The total number of states within each of these multiplets, including degeneracies, is 2^N.

3.2. *Ground state energies*

Figure 4 shows the dependence of the ground state energy per particle E_0/N on the particle number N for different L. The data are multiplied by L in order to eliminate the trivial L dependence. The charging model would yield a straight line for the ground state energy as a function of the particle number $E_0(N)$ when plotted in the same way. In very small systems E_0/N deviates from a linear $(N-1)$-dependence due to the discreteness of the spectrum of H_0. On the other hand, for systems with large L the formation of an inhomogeneous charge density (Wigner molecule, see below) prevents the ground state energy of few electrons to obey $E_0/N \propto (N-1)$. A better approximation is obtained by considering the Coulomb energy of N point charges at equal distances

$$r_c = L/(N-1)\,.$$

The importance of this charge "crystallization", which is a consequence of the charge quantization, for the capacitance per unit length C/L can be visualized for equidistant elementary point charges in 1D. With $C(N) := (Ne)^2/2U$ and U given by the electrostatical energy one obtains

$$C(N)/L = \frac{N}{2(N-1)} \left[\sum_{j=2}^{N} \frac{1}{j} \right]^{-1} .$$

In contrast to the classical capacitance of a long and homogeneously charged cylinder, this capacitance per unit length is independent of L but explicitly dependent on the charge. Thus it is not a constant. Also in higher dimensionalities we expect considerable fluctuations of the capacitance as a function of the charge due to the inhomogeneity of the charge density.

On the other hand for short systems with a more homogeneous charge distribution, quantum mechanical corrections to the ground state energy lead to the non-applicability of the capacitance formula. Our ground state energies cannot be reproduced by adding $(Ne)^2/2C$ to the ground state of the non-interacting system.

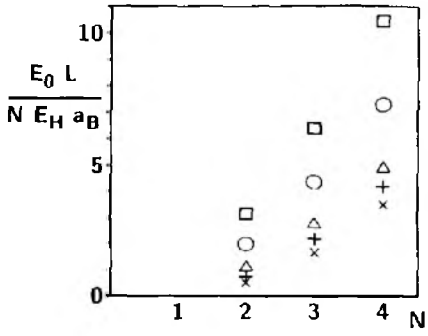

Fig. 4. Ground state energies per particle E_0/N multiplied by L/a_B versus the particle number N for: $L = 6.61a_B$ (□); $L = 16.1a_B$ (○); $L = 94.5a_B$ (△); $L = 944.8a_B$ (+). (×) denote the energy of N fixed point charges equally spaced at distances $L/(N-1)$. The quantum mechanical ground state energies (slowly) approach these values as $L \to \infty$.

3.3. *Wigner molecule*

The formation of localized charge density distributions with increasing electron distance is visualized by the one-particle density

$$\rho(x) = \sum_{\sigma} \langle \psi_G^{(N)} | \Psi_\sigma^\dagger(x) \Psi_\sigma(x) | \psi_G^{(N)} \rangle$$

for the N-electron ground state $|\psi_G^{(N)}\rangle$ at a certain system length L, as it is provided from the diagonalization of our model Hamiltonian (6). The field operator $\Psi_\sigma^\dagger(x)$ is defined to create one electron with spin σ at the position x. The truncation of the Hilbert space restricts the n summation over the eigenfunctions $\varphi_n(x)$ of the non-interacting (confinement) problem H_0 to $\Psi_\sigma^\dagger(x) = \Sigma_{n=1}^{M} \varphi_n(x) c_{n,\sigma}^\dagger$.

In fig. 5 $\rho(x)$ is shown for three electrons and

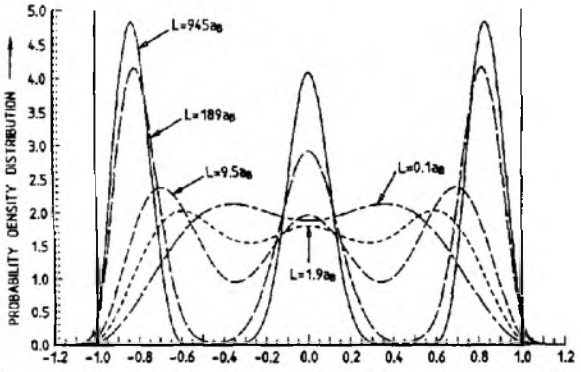

Fig. 5. One-particle density $\rho(x)$ of three electrons for different system lengths. The abscissa is rescaled to the interval $[-1, 1]$ as described in the text. To obtain the ground state $|\psi_G^{(3)}\rangle$ the lowest $M = 13$ single particle eigenfunctions have been taken into account. The transition from a weak influence of the Coulomb interaction to the fully established Wigner molecule can be followed for $0.1a_B \leq L \leq 945a_B$. Already for $L \geq 1a_B$ three peaks begin to develop. For $L \geq 100a_B$ the peaks are well separated, the charge in-between being nearly vanishing.

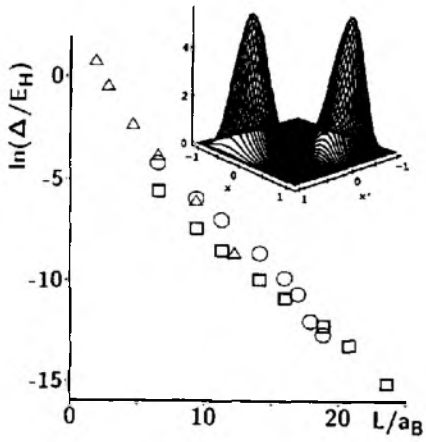

Fig. 6. The logarithm of the energy difference Δ between the ground state and the first excited state within the lowest multiplet is shown versus the system length for $N = 2$, $M = 11$ (□), $N = 3$, $M = 13$ (○), and $N = 4$, $M = 10$ (△). From the slope we estimate $L_\lambda \approx 1.5a_B$. As inset, the pair correlation function $\rho_C(x, x')$ is presented as it is defined in eq. (8) for $N = 2$ and $L = 19a_B$. The two coordinates are normalized to the interval $[-1, 1]$.

various system lengths. In order to allow comparisons, the length scale on the abscissa is normalized to the interval $[-1, 1]$ and the ordinate is correspondingly rescaled to leave the integral $\int dx\, \rho(x) = 3$ invariant. For later purposes a finite height of the potential barrier V/L^2 has been considered which is of no qualitative relevance here besides the fact that the one particle density does not vanish outside the square well box in fig. 5.

For $L \leq 0.1a_B$, the Coulomb interaction in eq. (6) is strongly suppressed and the charge density resembles the non-interacting case. Two of the electrons are in the first quantum state (with opposite spin) which is an even function of x and the third one populates the second quantum state, causing the dip at $x = 0$. Already at $L \geq 1a_B$ the three maxima start to develop. This length scale very well corresponds to the transition from non-interacting properties of the system to the strongly Coulomb dominated tunneling behavior for the low lying excitations as it will be described in section 3.4. Further increase of L eventually leads to a nearly vanishing charge density between the positions of the maxima. For $r_s \geq 100a_B$ the Wigner molecule is fully established and the ground state energy may be approximated by three elementary charges at a distance r_s.

The pair correlation function

$$\rho_C(x, x') = \sum_{\sigma,\sigma'} \langle \psi_G^{(N)} | \Psi^+_\sigma(x) \Psi^+_{\sigma'}(x') \Psi_{\sigma'}(x') \Psi_\sigma(x) | \psi_G^{(N)} \rangle \quad (8)$$

for $N = 2$ is shown in the inset of fig. 6. ρ_C is related to the density–density correlation function through $\rho_2(x, x') = \rho(x)\delta(x - x') + \rho_C(x, x')$. ρ_C gives the probability to find an electron at the position x when the second electron is supposed to be at x'. For two particle states from the lowest multiplet, in contrast to the non-interacting case, this correlation function is not very sensitive to the total spin of the wave function. In this case each of the peaks resemble the square of the pocket states described in section 3.4.

3.4. Low lying excitations

For $L \gg Na_B$ the spectrum of the low lying excitations can be understood using the picture

of a Wigner molecule. The one particle density shows N approximately equidistant peaks [25]. One type of excitation in such an arrangement is of a phonon kind due to the Coulomb forces between the charges. Similar to the one particle density these *vibrational* excitations are insensitive to the total spin and the symmetry properties of the wave function. The typical phonon frequencies Ω decrease with increasing system length, this is also found from our numerical eigenvalues. The decrease can be approximated asymptotically by $\Omega \sim r_s^{-\gamma}$ [26] at electron distances $r_s \geq 100 a_B$. Then the 1D Wigner molecule in the previous section is found to be fully established.

Already for much higher electron densities the lowest eigenvalues show the characteristic property of level multiplets (fig. 3), each containing 2^N states. The energy distance between the multiplets corresponds to the vibrational excitations, whereas the comparatively narrow fine structure determines the *tunneling* kind of excitations.

This fine structure spectrum can be understood by considering the N-dimensional configuration space L^N [27]. Due to the symmetry of the potential (5), the modulus of the N-particle probability amplitude has maxima at $N!$ different points corresponding to the number permutations of N particles. The eigenfunctions can approximately be identified with linear combinations of "pocket states" $|j\rangle$, $1 \leq j \leq N!$, each being concentrated around the vicinity of one potential minimum. The coefficients for the linear combination are determined by the irreducible representations of the associated permutation group. Correspondingly the eigenvalues are approximated by eigenvalues of a $N!$-dimensional Hamiltonian matrix. Their differences are proportional to overlap integrals between the states $|j\rangle$. From these suppositions, the relative distances between the fine structure levels can be determined using group theoretical arguments [27]. Assuming an asymptotically exponential decay of the pocket state wave functions suggests that $\Delta \propto \exp(-L/L_\Delta)$, where Δ is the energy difference between the ground state and the first excited state within the lowest multiplet. L_Δ is then a characteristic length scale beyond which the non-interacting spectrum is changed into the multiplet structure characteristic for the influence of the Coulomb interaction. In fig. 6 the L-dependence of $\ln(\Delta/E_H)$ is plotted for different N. From the slope of the linear part of the data we obtain $L_\Delta \approx 1.5 a_B$.

4. Conclusions

We have found that the AC conductance of a quantum mechanical tunnel barrier can be simulated in a certain range of parameters by a classical circuit. This correspondence can be used to define a dynamical quantum mechanical capacitance of the tunnel contact. The latter depends not only on geometrical parameters like a classical capacitance but also on Fermi energy and effective mass of the charge carriers. Like the tunnel resistance the dynamical capacitance is of quantum mechanical origin. This was demonstrated using a model with electron–phonon interaction destroying quantum mechanical coherence.

We have further argued that the dynamical capacitance should not depend on the Coulomb interaction above a critical frequency ω_0. Thus if the capacitance is a genuine property of the system independent of the experiment which is used for its detection one may conclude that the dynamical capacitance has to be the same as the static capacitance used for the explanation of Coulomb blockade experiments.

The frequency ω_0 can also be considered to be an upper limit for the observation of the Coulomb blockade effect and, important for practical applications, the limiting frequency for turnstile devices [28,29] proposed as current standard. Reasonable parameter values for GaAs–AlGaAs structures [6] ($V = 0.75$ meV, $E_F = 0.05$ meV, $m = 0.07 m_e$, $b = 130$ nm and $l = 1$ μm) yield $\omega_0 \approx 1$ GHz. This would limit the highest achievable current in such a turnstile device to about 25 pA. Using the estimate [29], $\omega_c = 2\pi/R_T C \sim T/C$, one obtains a frequency which is an order of magnitude smaller.

Furthermore, we have calculated numerically

the energy spectra of up to $N = 4$ electrons confined in a quasi-one-dimensional square well potential of finite length. The discussion in terms of the pocket state basis suggests that our presented classification of the energy eigenvalues should remain valid also in 2D or 3D systems if the width of the system does not exceed the width of one pocket state wave function. Our $N = 2$ eigenvalues agree nearly quantitatively with the lowest eigenvalues calculated by Bryant [30] in a rectangular two dimensional quantum dot, which has been 10 times longer than wide.

We have demonstrated that the ground state energies $E_0(N)$ deviate from the N^2 behavior assumed in the charging model because of the formation of a Wigner-molecule-like structure at sufficiently low electron densities (quantization of the charge) and the quantum mechanical influence of the kinetic energy (non-commutativity of H_0 and H_1). Only in sufficiently large systems *and* at sufficiently high electron densities, a capacitance-like behavior can be obtained.

We have obtained three different regimes for the electron densities to characterize the excitation spectra. The Wigner molecule is found to be fully established for densities $1/r_s$ below $10^{-2} a_B^{-1}$. Nevertheless, the description of the interacting spectrum in terms of the pocket state picture does already hold at much larger electron densities. Note that the pocket states are collective modes of all electrons. The reason is shown to be the onset of the peak structure of the charge density already for much shorter systems (fig. 5). Only for $L \lesssim L_\Delta \approx 1.5 a_B$ the confinement energy starts to dominate the Coulomb energy and the spectrum approaches the non-interacting limit (fig. 6). Neither the ground state energy nor the level spectrum is given by a sum of kinetic and potential energy eigenvalues separately!

Experiments are frequently performed on AlGaAs/GaAs-based heterostructures which rather correspond to a 2D situation. It is not obvious in how far our 1D classification for the length and energy scales of few Coulombically interacting electrons can be applied to that case. If we assume that at least the qualitative aspects of our classification into different regimes for the electron density can be used, the intermediate regime should apply in most circumstances. Given the geometry and the electron numbers in typical quantum dots [5] (area of the dot $\approx 10^5\,\mathrm{nm}^2$, number of electrons $\approx 10^2$, effective mass $\approx 0.07 m_e$, dielectric constant ≈ 10) a mean distance of $r_s \approx 3 a_B$ can be estimated. For this relatively high electron density the *ground state energy*, which is in first approximation the relevant quantity that enters a linear DC transport experiment, can roughly be estimated by using the charging model. However, the *excitation energies* in quantum dots can never be found by just adding the (non-interacting) confinement energy levels. They are substantially characterized by the fine structure level spectrum differing e.g. in total spin.

In experimental situations as they were recently realized by Meurer et al. [13] with only a few electrons per quantum dot, the charging model cannot be expected to yield correct results for the ground state energy.

Acknowledgements

It is a pleasure to acknowledge fruitful discussions with Hermann Grabert, Peter Hänggi, Gert Ingold, Gerd Schön, Uli Weiss and all the participants of the 1992 Tankum seminar and the Sion workshops. We also thank the PTB theory group, in particular Walter Apel. This work was supported in part by the Deutsche Forschungsgemeinschaft via the grants AP 47/1-1, We 1124/4-1 and Sonderforschungsbereich 345, and within the SCIENCE program by the Commission of the European Communities, contract number SCC-CT90-0020.

References

[1] B. Kramer (ed.), Quantum Coherence in Mesoscopic Systems, NATO ASI Series B 254 (Plenum Press, New York, 1991).

[2] D.V. Averin and K.K. Likharev, in: Mesoscopic Phe-

nomena in Solids, eds. B.L. Altshuler, P.A. Lee and R.A. Webb (North-Holland, Amsterdam, 1991);
G. Schön and A.D. Zaikin, Phys. Rep. 198 (1990) 237;
H. Grabert, G.-L. Ingold, M.H. Devoret, D. Esteve, H. Pothier and C. Urbina, Z. Phys. B 84 (1991) 143;
T.A. Fulton and G.J. Dolan, Phys. Rev. Lett. 59 (1987) 109.

[3] H. Grabert (ed.), Special Issue on Single Charge Tunneling, Z. Phys. B 85 (1991) 317.

[4] D.V. Averin and K.K. Likharev, J. Low Temp. Phys. 62 (1986) 345;
P. Delsing, K.K. Likharev, L.S. Kuzmin and T. Claeson, Phys. Rev. Lett. 63 (1989) 1861.

[5] U. Meirav, M.A. Kastner and S.J. Wind, Phys. Rev. Lett. 65 (1990) 771;
L.P. Kouwenhoven, N.C. van der Vaart, A.T. Johnson, W. Kool, C.J.P.M. Harmans, J.G. Williamson, A.A.M. Staring and C.T. Foxon, in ref. [3] p. 367;
M.A. Kastner, Rev. Mod. Phys. 64 (1992) 849.

[6] Y. Meir, N.S. Wingreen and P.A. Lee, Phys. Rev. Lett. 66 (1991) 3048;
Y. Meir and N.S. Wingreen, Phys. Rev. Lett. 68 (1992) 2512.

[7] L.P. Kouwenhoven, PhD thesis, University of Delft (1992), which contains a collection of papers on this subject.

[8] D.V. Averin and G. Schön, in ref. [1] p. 531.

[9] C.W.J. Beenakker, Phys. Rev. B 44 (1991) 1646.

[10] U. Eckern, G. Schön and V. Ambegaokar, Phys. Rev. B 30 (1984) 6419.

[11] W. Häusler, B. Kramer and J. Mašek, in ref. [3] p. 435.

[12] A.T. Johnson, L.P. Kouwenhoven, W. de Jong, N.C. van der Vaart, C.J.P.M. Harmanns and C.T. Foxon, Phys. Rev. Lett. 69 (1992) 1592.

[13] B. Meurer, D. Heitmann and K. Ploog, Phys. Rev. Lett. 68 (1992) 1371.

[14] F.W.J Hekking, Y.V. Nazarov and G. Schön, Europhys. Lett. 20 (1992) 255.

[15] D.S. Fisher and P.A. Lee, Phys. Rev. B 23 (1981) 6851.

[16] B. Velický, J. Mašek and B. Kramer, Phys. Lett. A 140 (1989) 447;
J. Mašek and B. Kramer, Z. Phys. B 75 (1989) 37;
B. Kramer and J. Mašek, Z. Phys. B 76 (1989) 457.

[17] G.D. Mahan, Many-Particle Physics (Plenum Press, New York, 1981).

[18] T. Brandes, D. Weinmann and B. Kramer, Europhys. Lett., to be published.

[19] R. Landauer, Phil. Mag. 21 (1970) 863;
M. Büttiker, Phys. Rev. Lett. 57 (1986) 1761.

[20] A.D. Stone and A. Szafer, IBM J. Res. Dev. 32 (1988) 384.

[21] E.N. Economou, Green's Function in Quantum Physics (Springer, Berlin, 1990).

[22] V. Špička, J. Mašek and B. Velický, J. Phys. Condens. Matter 2 (1990) 1569.

[23] J. Mašek and B. Kramer, Solid State Comm. 68 (1988) 611.

[24] P.A. Maksyms, T. Chakraborty, Phys. Rev. Lett. 65 (1990) 108;
U. Merkt, J. Huser, M. Wagner, Phys. Rev. B 43 (1991) 7320;
D. Pfannkuche, R.R. Gerhards, Phys. Rev. B 44 (1991) 13132;
V. Halonen, T. Chakraborty, P. Pietiläinen, Phys. Rev. B 45 (1992) 5980.

[25] K. Jauregui, W. Häusler and B. Kramer, to be published.

[26] W. Häusler and B. Kramer, Phys. Rev. B, to be published.

[27] W. Häusler, to be published.

[28] L.J. Geerligs et al., Phys. Rev. Lett. 64 (1990) 2691.

[29] M.H. Devoret et al., Bull. Bureau National de Métrologie 86 (1991) 7.

[30] G.W. Bryant, Phys. Rev. Lett. 59 (1987) 1140.